Globin-coupled heme containing oxygen sensor soluble adenylate cyclase in *Leishmania* prevents cell death during hypoxia

Sumit Sen Santara, Jayasree Roy, Supratim Mukherjee, Moumita Bose, Rina Saha, and Subrata Adak[1]

Division of Structural Biology and Bio-Informatics, Council of Scientific and Industrial Research-Indian Institute of Chemical Biology, Kolkata 700032, India

Edited by Paul R. Ortiz de Montellano, University of California, San Francisco, CA, and accepted by the Editorial Board September 2, 2013 (received for review March 4, 2013)

Globin and adenylate cyclase play individually numerous crucial roles in eukaryotic organisms. Comparison of the amino acid sequences of globins and adenylate cyclase from prokaryotic to eukaryotic organisms suggests that they share an early common ancestor, even though these proteins execute different functions in these two kingdoms. The latest studies of biological signaling molecules in both prokaryotic and eukaryotic organisms have discovered a new class of heme-containing proteins that act as sensors. The protein of the globin family is still unknown in the trypanosomatid parasites, *Trypanosome* and *Leishmania*. In addition, globin-coupled heme containing adenylate cyclase is undescribed in the literature. Here we report a globin-coupled heme containing adenylate cyclase (HemAC-Lm) in the unicellular eukaryotic organism *Leishmania*. The protein exhibits spectral properties similar to neuroglobin and cytoglobin. Localization studies and activity measurements demonstrate that the protein is present in cytosol and oxygen directly stimulates adenylate cyclase activity in vivo and in vitro. Gene knockdown and overexpression studies suggest that O_2-dependent cAMP signaling via protein kinase A plays a fundamental role in cell survival through suppression of oxidative stress under hypoxia. In addition, the enzyme-dependent cAMP generation shows a stimulatory as well as inhibitory role in cell proliferation of *Leishmania* promastigotes during normoxia. Our work begins to clarify how O_2-dependent cAMP generation by adenylate cyclase is likely to function in cellular adaptability under various O_2 tensions.

Human pathogen *Leishmania* promastigotes inhabit the midgut of a sandfly, where they are densely packed together and the environment of these promastigotes is then likely to become hypoxic or even anoxic (1). Although biologists have long known that *Leishmania* species can survive under limited oxygen (2), the underlying mechanism remains unclear.

O_2, CO, and NO are physiologically indispensable but sometimes toxic to living organisms (3). Hence, the machinery for sensing these molecules and responding to them is vital for survival. Recently, a new class of the heme-containing sensor proteins has been discovered (4). These are different from well-known heme proteins, such as O_2 carriers (hemoglobin/myoglobin), oxygen activators (cytochrome P450/peroxidases), and mediators of electron transfer (cytochrome *c*/cytochrome b_5) (5, 6). Heme-based sensor proteins usually consist of an N-terminal heme-containing sensor domain and a C-terminal effector domain (7). The structures of heme-based sensor proteins are changed upon binding of O_2, CO, or NO gases with the heme domain. This structural change influences the effector domain for proper functioning.

Cyclic AMP (cAMP) is a vital signaling molecule that controls diverse biological functions in many organisms, including virulence factors from a range of pathogens (8, 9). The second messenger cAMP is universally generated by adenylate cyclase (AC), which catalyzes the cyclization of ATP to cAMP. AC is regulated by various molecules including bicarbonate (10), calcium (11), and hormones (12). Although cAMP is found in the trypanosomatid parasite *Leishmania,* little is known about its function (13, 14).

In this paper we report the heme containing AC from *Leishmania major* (HemAC-Lm). To understand the biochemical functions of this protein, we cloned, expressed, and characterized the HemAC-Lm protein. Evidence has been presented to show that a globin domain present at the N terminus of HemAC-Lm plays an important role in O_2 binding and controls the catalytic activity of the C-terminal AC domain. Our results provide evidence for the existence of an O_2-dependent cAMP regulation that is a prerequisite for decreasing oxidative stress under hypoxia.

Results and Discussion

Primary Structure of HemAC-Lm Protein. Eleven ACs were predicted in the *L. major* genome-sequencing project. One of the predicted 11 ACs (systematic name: LmjF.28.0090), comprising 616 residues, exhibits two striking features: first, its N terminus (residues 85–209) displays limited homology to globin (Fig. S1) and second, the C terminus (residues 360–616) bears 27% homology with the class III adenylate/guanylate cyclase (Fig. S1). The absolutely conserved residues of all globins are the proximal His in the F helix, Pro in C helix, and Phe in the CD1 region (15). All three residues, Pro115, Phe121, and His161, are conserved in this protein (Fig. S1). The C terminus of this gene carries an AC characteristic lysine (Lys-427) and aspartic acid (Asp-508) residues (16). These features suggested to us that this AC might

Significance

Heme protein sensors interact with various gaseous molecules, such as CO, NO, or O_2, and play a crucial role in transcriptional and regulatory events. In general, the sensory domains of heme proteins control signal transduction domains such as histidine kinases, phosphodiesterases, DNA-binding domains, guanylate cyclases, diguanylate cyclase, and aerotaxis transducers. Here we report globin-coupled heme containing adenylate cyclase from *Leishmania major* (HemAC-Lm), which regulates O_2-dependent cAMP synthesis. Oxygen binding at heme iron of HemAC-Lm presumably triggers a conformational change in the sensor domain that sequentially stimulates the catalytic activity of the adenylate cyclase domain, resulting in the synthesis of the second messenger cAMP. This O_2-dependent cAMP signaling is likely to function in cellular adaptability during hypoxia.

Author contributions: S.S.S. and S.A. designed research; S.S.S., J.R., S.M., M.B., R.S., and S.A. performed research; S.A. analyzed data; and S.A. wrote the paper.

The authors declare no conflict of interest.

This article is a PNAS Direct Submission. P.R.O.d.M. is a guest editor invited by the Editorial Board.

[1]To whom correspondence should be addressed. E-mail: adaks@iicb.res.in.

This article contains supporting information online at www.pnas.org/lookup/suppl/doi:10.1073/pnas.1304145110/-/DCSupplemental.

be a globin-coupled heme containing an AC protein (HemAC-Lm) that generates signals in response to binding of oxygen.

Biochemical and Spectral Characteristics of HemAC-Lm. To identify the biochemical characteristics of HemAC-Lm, both the full-length protein and truncated catalytic domain (Δ360 HemAC-Lm, 360 amino acid deleted from the N terminus) were expressed in *E. coli*. Purified HemAC-Lm and Δ360 HemAC-Lm migrated to positions as expected from the theoretical relative molecular mass of 72 kDa (Fig. 1*A*, lane 4) and 30 kDa protein (Fig. 1*A*, lane 9), respectively. Fig. 1*B* showed that both HemAC-Lm and Δ360 HemAC-Lm proteins were dimeric, indicating that the N-terminal 360 amino acids were not responsible for dimerization. Antiglobin domain of HemAC-Lm (1-209 aa) antisera detected the 68-kDa mature form of HemAC-Lm in cytosolic fraction of *Leishmania* lysate (Fig. 1*C*). HemAC-Lm displayed absorption spectra characteristic of oxygen-bound heme proteins (Fig. 2*D*). Absorption maxima were observed at 414 (Soret), 575 (α-band), and 538 nm (β-band) for HemAC-Lm proteins, compared with corresponding maxima of 414, 576, and 538 nm for oxyhemoglobin (Fig. 2*D*) (17). The deoxygenated form of the HemAC-Lm protein shifted the Soret band from 414 to 423 nm, and simultaneously, the αβ-band appeared at 560 and 532 nm (Fig. 1*D*). This behavior is consistent with the formation of ferrous six-coordinate low-spin heme and is also seen with deoxyneuroglobin/deoxycytoglobin (18). HemAC-Lm binds with CO, and new peaks appear at 419 (Soret), 573 (α-band), and 535 nm (β-band) (Fig. 1*D*), indicating that the native form of HemAC-Lm is in the ferrous state. HemAC-Lm catalyzed only the conversion of ATP to cAMP (Fig. 1*E*). The activity was insensitive to transmembrane AC activator (forskolin) and soluble AC inhibitor (KH7), suggesting that HemAC-Lm is unlikely to be transmembrane AC or bicarbonate-stimulated soluble AC (Fig. 1*E*). We measured AC activity in the presence or absence of common gaseous sensor (O_2 and CO) molecules under anaerobic condition (Fig. 1*E*). The O_2- or CO-bound protein showed AC activity, indicating that activation was due to binding of the molecule with heme. The K_m value for ATP of this enzyme is ∼1.9 mM (Fig. 1*F*). O_2-dependent spectral shift and AC activity (Fig. 1 *G* and *H*) suggest that AC activity is directly proportional to the conversion of the oxy form of enzyme.

Characteristics of Overexpressing, Control, Heterozygous Knockout, and Tetracycline Inducible Knockdown Cells During Normoxia. To investigate the physiological role of HemAC-Lm, we constructed tetracycline inducible knockdown (IKO), heterozygous knockout (HKO), and overexpressing (OE) cell strains. The null mutant cell line was unable to proliferate in culture media under normoxia. HemAC-Lm protein was 85% and 50% lower in IKO and HKO cells, respectively, and expressed ∼2.3 times higher in OE cells compared with control (CT) cells (Fig. 2*A*). Like HemAC-Lm expression, the order of intracellular cAMP accumulation was OE > CT > HKO > IKO cells (Fig. 2*B*). The protein kinase A (PKA) activity was higher in OE cells and lower in HKO or IKO cells compared with CT cells (Fig. 2*C*), indicating that elevated cAMP activates PKA activity. To investigate whether the O_2 consumption rate is changed with the changing cAMP level in OE, CT, HKO, or IKO cells, we measured O_2 consumption rate in all types of cells. Fig. 2*D* shows that the O_2 consumption rates are directly proportional to the intracellular cAMP concentration. Like our results, earlier researchers showed that the O_2 consumption rate increased in response to increasing cAMP level (19). OE, IKO, or HKO populations had slower growth rates compared with CT cells (Fig. 2*E*), revealing dual, bidirectional effects of cAMP on *Leishmania* growth. To strengthen the above results, we measured the growth rate of HKO cells in the presence of different concentrations of 8-bromocAMP (Fig. 2*F*). The data confirmed that the effect of cAMP on cell proliferation

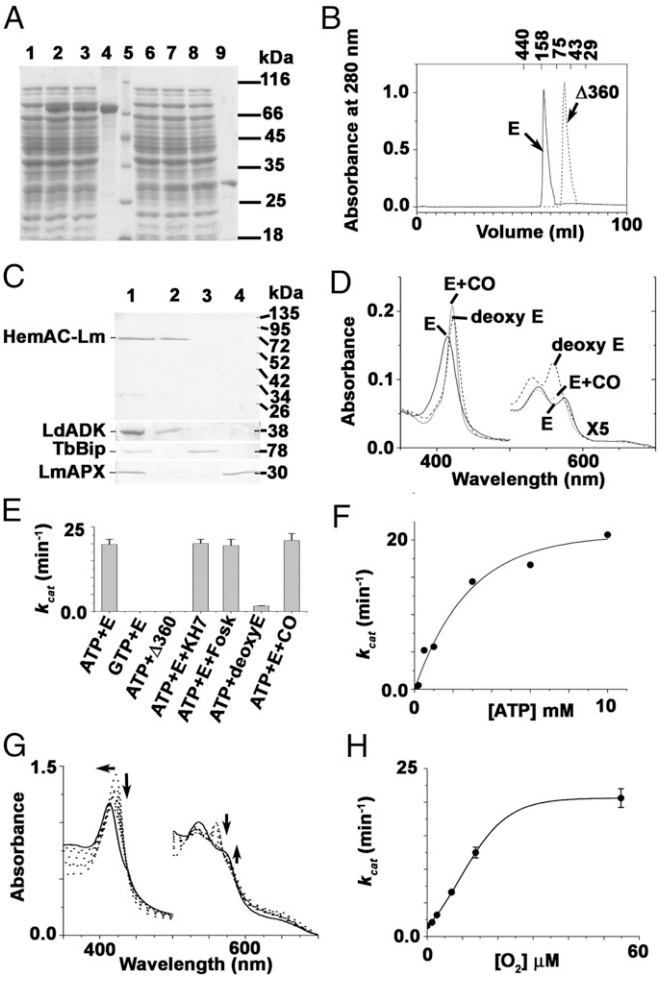

Fig. 1. Biochemical characteristics of HemAC-Lm. (*A*) SDS/PAGE. Lanes: 1, −isopropyl β-D-1-thiogalactopyranoside (IPTG) (full length); 2, +IPTG (full length); 3, lysate flow through (full length); 4, purified full-length protein; 5, molecular weight marker; 6, −IPTG (Δ360); 7, +IPTG (Δ360); 8, lysate flow through (Δ360); and 9, purified (Δ360). (*B*) The size exclusion chromatography of purified full-length and truncated proteins by using Superdex 200 Columns of ÄKTAprime plus system (GE Healthcare). (*C*) Subcellular localization was performed using rabbit anti–HemAC-Lm primary antibody. Lanes: 1, whole cells; 2, cytosolic fraction; 3, endoplasmic reticulum (ER) fraction; and 4, mitochondrial fraction. Marker proteins *Leishmania donovani* adenosine kinase, *T. brucei* Bip, and *L. major* ascorbate peroxidase were used in the subcellular fractions as cytosolic, ER, and mitochondrial markers, respectively. (*D*) Electronic absorption spectra of 1.6 μM HemAC-Lm in 50 mM Tris·HCl buffer, pH 7.4. The solid line, dashed line, and dotted line represent the spectra of the native, +dithionite, and +CO, respectively. (*E*) AC activity in the presence of activator and inhibitor. The concentrations of ATP, GTP, full-length HemAC-Lm (E), Δ360HemAC-Lm (Δ360), KH7, and foskolin used were 5 mM, 5 mM, 100 μg, 150 μg, 50 μg, and 100 μg, respectively. (*F*) ATP-dependent cAMP production. (*G*) O_2-dependent spectral shift of deoxy enzyme by sequential addition of 1.4, 2.8, 7, 14, and 56 μM O_2. (*H*) O_2-dependent AC activity.

was bidirectional. A similar type of bidirectional response of cAMP is also observed in other types of cells (20, 21). To further substantiate the growth arrest in the HKO, IKO, or OE cells compared with CT cells, cellular DNA content was estimated in parallel by flow cytometry (Fig. 2*G* and Fig. S2); the results clearly confirmed the data obtained from the growth curve (Fig. 2*E*). The progression of the cell cycle was significantly delayed in OE, IKO, or HKO cells where the generation time was greater than 12 h, compared with CT cells having generation time of 8 h

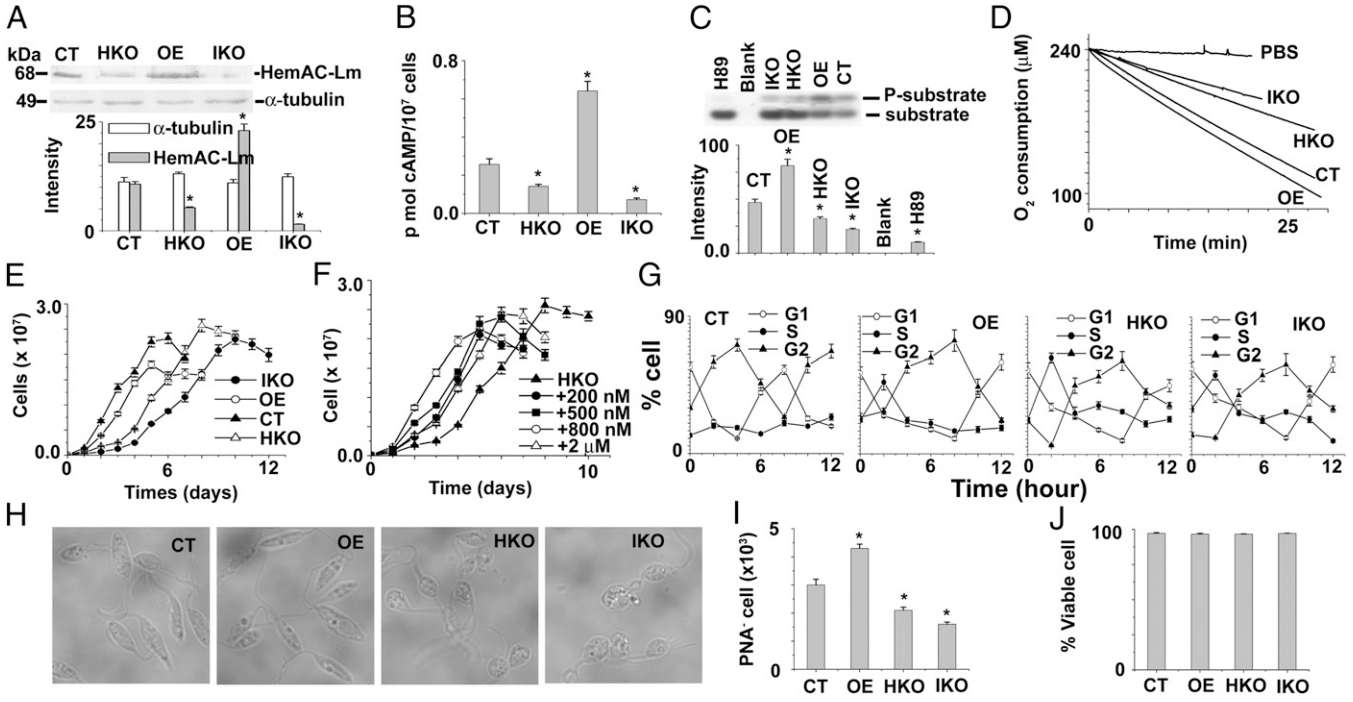

Fig. 2. Functional characterization of HemAC-Lm during normoxia. (*A*) Western blot results using anti–HemAC-Lm and anti–α-tubulin antibody. Fifty micrograms of *L. major* lysate were used for Western blotting. All of the data are representative of at least three independent experiments. (*B*) Intracellular cAMP content in CT, OE, HKO, and IKO cells. (*C*) Intracellular PKA activity in CT, OE, HKO, and IKO cells. The concentration of H89 (PKA inhibitor) used is 100 μM. UV-illuminated 0.8% agarose gels after electrophoresis are shown at the top. Upper and lower bands are denoted phosphorylated and non-phosphorylated PepTag peptides, respectively. (*D*) The O_2 consumption rate in CT, OE, HKO, and IKO cell lines. (*E*) The growth curves of CT, OE, HKO, and IKO cells. (*F*) The growth curve of HKO cells in the presence of different concentrations of Br-cAMP. (*G*) The cell cycle distribution of CT, OE, HKO, and IKO cell lines after removing the hydroxyurea block. (*H*) The changing morphology of log-phase *Leishmania* promastigotes with the changing levels of endogenous HemAC-Lm gene. (*I*) The PNA negative log-phase *Leishmania* promastigotes in CT, OE, HKO, and IKO cell lines. (*J*) The viable cell (propidium iodide- and annexin V-negative cell) analyzed by flow cytometer in CT, OE, HKO, and IKO cell lines. All values shown are means ± SD of three independent experiments. Asterisks indicate statistically significant values of less than 0.05.

(Fig. 2*G* and Fig. S2). These results strongly indicated that the normal level of cAMP plays a positive role, whereas an excess of cAMP plays a negative role in the initiation of cell proliferation under normoxia. The IKO and HKO populations had a distinct type of cell morphology compared with OE cells; that is, the OE population had more cells that are slender and elongated in shape, whereas the IKO or HKO cells are mostly round shaped (Fig. 2*H*). Because the morphology of infectious metacyclic stage of cells is slender (22, 23), we quantitated metacyclic promastigotes by negative agglutination with peanut agglutinin (PNA). Flow cytometry results showed that OE culture had ∼1.5-fold excess metacyclic (PNA^-) parasites compared with CT, HKO, or IKO cells (Fig. 2*I*). These results suggest that the excessive cAMP accumulation in OE cells causes growth arrest, and subsequently, the cell differentiates from procyclic to metacyclic stage. A similar type of result has been reported in *Trypanosoma brucei* (24), where they have shown that excessive cAMP causes a growth arrest and cell differentiation from procyclic to infective stage. Because the typical apoptotic morphology of a cell is round, we suspected that HKO or IKO culture might have higher levels of apoptotic cells. However, the HKO or IKO culture had greater than 98% viable cells [annexin V- and propidium iodide (PI)-negative cells], which was similar to CT cell (Fig. 2*J*), indicating that the round-shaped cells were not apoptotic cells.

Characteristics of OE, CT, HKO, and IKO Cells During Hypoxia. To investigate the implication of O_2 dependence in AC activity, cells were incubated under hypoxia. The cAMP accumulation in hypoxic CT cells (Fig. 3*A*) was lower than normoxic CT cells (Fig. 2*B*), indicating that suppressing cAMP level during hypoxia might be an essential factor for cell survival. Like aerobic organisms, oxygen depletion for 12 h resulted in a 70% decrease of ATP levels (Fig. 3*B*) in comparison with normoxia (25). As shown in Fig. 3*B*, the ATP levels of all types of cells are similar during hypoxia, irrespective of their different levels of intracellular HemAC-Lm. Flow cytometry (Fig. 3*C*) and microscopic (Fig. 3*D*) studies suggest that HKO, IKO, and OE cells had ∼30–40% cell death (PI- or annexin V-positive cells), whereas control cells had 10% cell death. For authentication of the above results, we measured the percentage of cell death in the presence or absence of different concentrations of CPT-cAMP and PKA inhibitors (H89 and PKI) (Fig. 3 *E*–*G*). During hypoxia, HKO or IKO results suggest that HemAC-Lm is an essential gene, but OE results suggest that excessive cAMP is toxic to the cell.

The question immediately arises of what mechanism is apparently involved in cell death during hypoxia. One possibility is that the lower ATP generation might be the cause of cell death (26); another option is that the generation of reactive oxygen species (ROS) can lead to mitochondrial dysfunctions, which are implicated in cell death (23). The first option behind accelerated cell death in OE, HKO, or IKO cells during hypoxia can be ruled out (Fig. 3*B*). Earlier results in other cells (27) and the present results show that decreased O_2 concentration results in an appearance of oxidative stress (Fig. 3*H*). Our data demonstrate that ROS generation increases further in OE, HKO, and IKO cells compared with CT cells during hypoxia (Fig. 3*H*). This excessive ROS generation in OE, HKO, and IKO cells may be responsible for a higher percentage of cell death during hypoxia. The addition of antioxidants (such as reduced glutathione and *N*-acetyl-L-cysteine) attenuated this ROS and also abolished the

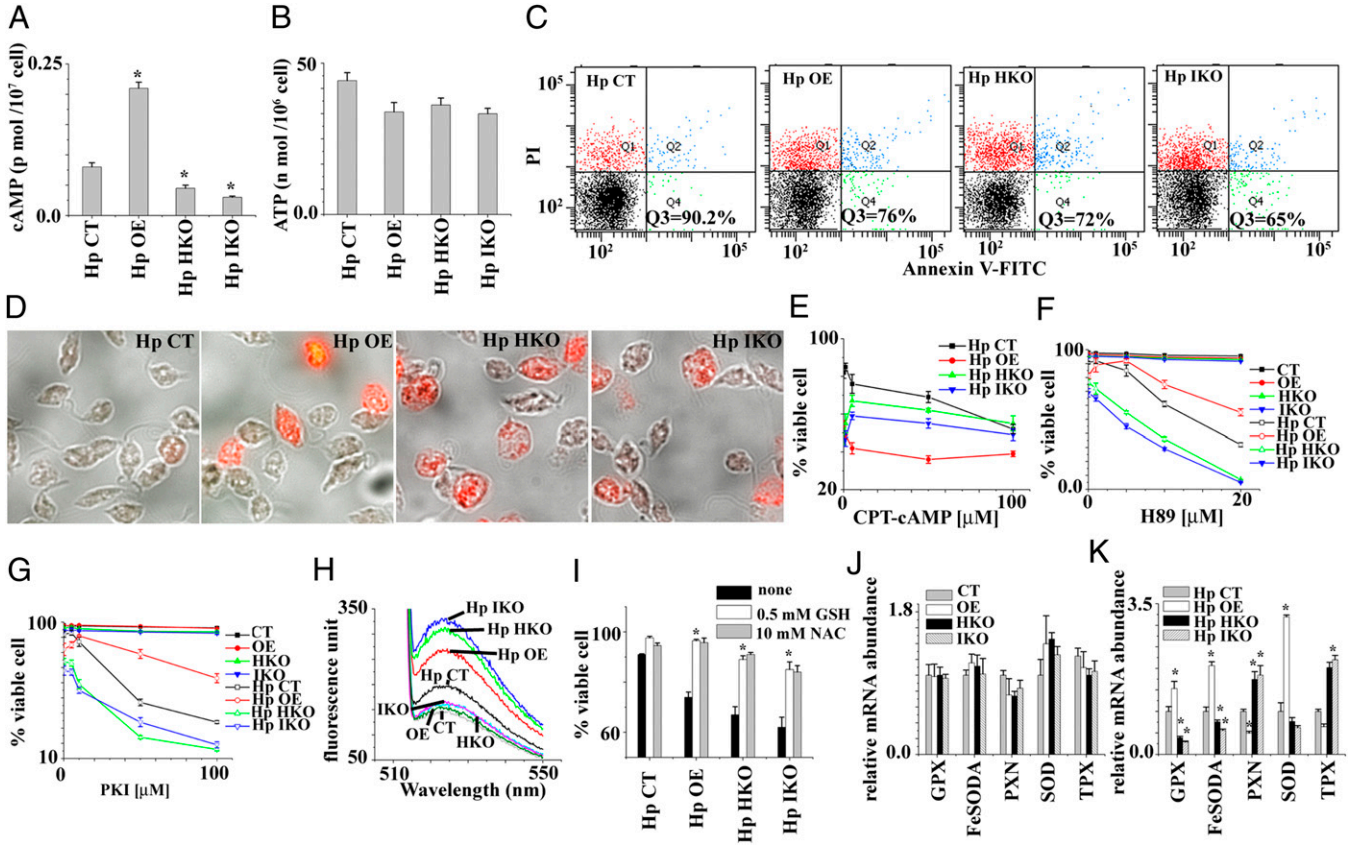

Fig. 3. Functional characterization of HemAC-Lm during hypoxia. (*A*) Intracellular cAMP content in CT, OE, HKO, and IKO cells after incubation of 12 h at hypoxic condition. Hp, hypoxic cell. (*B*) Intracellular ATP content in CT, OE, HKO, and IKO cells after incubation of 12 h at hypoxic condition. (*C*) The viable cell (propidium iodide- and annexin V-negative) analyzed by flow cytometer in CT, OE, HKO, and IKO cell lines after incubation for 12 h at hypoxic condition. Cells were double stained with annexin V and propidium iodide. Dot plots are divided into four quadrants. The lower left quadrant represents viable cells (annexin V- and PI-negative cell). All of the data are representative of three independent transfection experiments (three different clones). (*D*) Fluorescence microscopic picture of the same cells as in *C*. (*E*) The number of viable cells after incubation of 12 h at hypoxic condition in presence of different concentrations of 8-(4-Chlorophenylthio)adenosine-3′, 5′-cyclic monophosphate (CPT-cAMP). (*F*) The number of viable cells after incubation of 12 h at hypoxic condition in presence of different concentrations of PKA inhibitor (H89). (*G*) The number of viable cells after incubation for 12 h at hypoxic condition in presence of different concentrations of protein kinase inhibitor (PKI). (*H*) Intracellular ROS analyzed by using fluorometer in CT, OE, HKO, and IKO cells after incubation of 12 h under normoxic and hypoxic condition. (*I*) The effect of antioxidants on cell survival during hypoxia. GSH, reduced glutathione; NAC, *N*-acetyl-L-cysteine. (*J*) The mRNA expression in CT, OE, HKO, and IKO cells after incubation of 12 h under normoxia. GPX, FeSOD, PXN, SOD, and TPX denote non-selenium glutathione peroxidase (LmjF.26.0810), iron superoxide dismutase A (LmjF08.0290), peroxidoxin peroxidase (LmjF23.0040), superoxide dismutase (LmjF30.2770), and tryparedoxin peroxidase (LmjF.15.1120), respectively. (*K*) The mRNA expression in CT, OE, HKO, and IKO cells after incubation of 12 h under hypoxia. Asterisks indicate statistically significant values of less than 0.05.

acceleration of cell death seen during hypoxia (Fig. 3*I*). Overall results suggest that O_2-dependent cAMP generation in control cells protects cells against the accelerated rates of cell death by suppressing excessive generation of cellular oxidative stress. Then what is the reason behind increased ROS production in OE, HKO, and IKO cells during hypoxia? The factors that control the rate of ROS generation by OE, HKO, and IKO cells are completely unknown but likely include the reduction of the antioxidant protein production. The cAMP-dependent activated PKA can phosphorylate a variety of substrates, thus explaining the broad range of cAMP effects. It is well known that the antioxidant gene transcription during oxidative stress condition varies because cAMP plays a dual role: intracellular cAMP induces the transcription of superoxide dismutase (28, 29) and represses the transcription of thioredoxin mRNA (30). To investigate the relative quantities of antioxidant genes in CT, OE, HKO, and IKO cells, we performed quantitative real-time PCR to measure non-selenium glutathione peroxidase (LmjF.26.0810), iron superoxide dismutase A (LmjF08.0290), peroxidoxin peroxidase (LmjF23.0040), superoxide dismutase (LmjF30.2770), and tryparedoxin peroxidase (LmjF.15.1120). Although quantitative real-time PCR results demonstrated approximately similar mRNA expression of antioxidant genes in all type of cells during normoxia (Fig. 3*J*), the level of mRNA expression of antioxidant genes was altered in different cell types during hypoxia (Fig. 3*K*). The higher level of cAMP containing OE cell showed increased levels of mRNA expression of iron superoxide dismutase A, superoxide dismutase, and non-selenium glutathione peroxidase. In contrast, the lower level of cAMP containing HKO or IKO cells revealed higher levels of mRNA expression of peroxidoxin peroxidase and tryparedoxin peroxidase. Thus, these results strongly suggest that the transcription of antioxidant genes is tightly regulated by HemAC-generated cAMP during hypoxia. Hence, O_2-dependent cAMP generation in control cells is an essential factor for keeping optimum levels of antioxidant gene transcription.

Conclusion. These data unequivocally demonstrate that AC activity can be regulated by the binding of O_2 to heme iron. HemAC proteins constitute a previously undescribed class of sensors that differ significantly from the known heme-containing O_2 sensors FixL (31), AxPDEA1 (32), NPAS2 (33), *Ec*DOS (3), DosC (34),

and HemAT-Bs (7). The heme-binding domain of FixL, AxPDEA1, NPAS2, and *Ec*DOS belongs to the PAS domain superfamily, but HemAC-Lm contains no PAS domain. In addition, HemAC-Lm regulates cAMP synthesis, whereas HemAT-Bs and DosC participate in aerotaxis and c-di-GMP generation, respectively. Therefore, HemAC differs from all oxygen sensor genes on the basis of physiological function. Our results suggest that the N-terminal domains of HemAC act as sensors by binding diatomic oxygen at their ferrous heme. The oxygen binding presumably triggers a conformational change in the sensor domain that, in turn, stimulates the activity of the C-terminal catalytic AC domain, resulting in the synthesis of the second messenger cAMP, which then associates with the gene transcription and cell survival under hypoxia.

Methods

Parasite Culture. Promastigote forms of *L. major* (strain 5ASKH) were grown at 26 °C in M199 medium supplemented with 40 mM Hepes (pH 7.4), 200 μM adenine, 1% penicillin–streptomycin (vol/vol), 50 μg/mL gentamycin, and 10% (vol/vol) heat-inactivated FBS.

Cloning, Expression, Purification, and Characterization of HemAC-Lm and Δ360HemAC-Lm. The coding region of full-length HemAC-Lm was PCR amplified from *L. major* genomic DNA, using primers 1 and 2 (Table S1). For the Δ360HemAC-Lm, the PCR amplification was carried out by using primers 3 and 4 (Table S1). The PCR products from two separate reactions were purified and cloned into the BamHI and XhoI sites of pTrcHisA (Invitrogen) for full-length HemAC-Lm and the BamHI and HindIII sites of pET16B (Novagen) for Δ360HemAC-Lm. A detailed description of the method for expression, purification, enzymatic assay, preparation of deoxy protein, subcellular fractionation, and Western blotting is provided in *SI Methods*. The concentration of protein was determined using Bio-Rad reagent with BSA as the standard. The heme was identified and quantified by the pyridine-hemochrome method (35). The molar extinction coefficient of full-length HemAC-Lm at 414 nm was 79,300 $M^{-1}{\cdot}cm^{-1}$.

UV-Vis Spectral Analysis. All spectral studies were performed at 25 ± 1 °C in a Shimadzu UV-2550 computerized spectrophotometer using quartz cells of 1 cm light path. Each set of experiments was done using freshly purified enzymes to avoid any spin state change due to freeze–thaw and storage of enzymes.

HemAC-Lm–Overexpressing Promastigotes. HemAC-Lm ORF was amplified using primers 5 and 6 (Table S1) and cloned into the SmaI- and BamHI-digested pXG-B2863 vector in the correct orientation to construct pXG:HemAC-Lm. pXG:HemAC-Lm was transfected in *L. major* promastigotes by electroporation as described earlier (36).

Generation of Stable Knockout Strain for HemAC-Lm Alleles. To generate the constructs pXG-NEO HemAC-Lm and pXG-HYG HemAC-Lm, 1.007 kb from the 5′ region and 1 kb from the 3′ region of HemAC-Lm gene were inserted into the modified pXG-NEO and pXG-HYG vectors (35), respectively. A detailed description of this method is provided in *SI Methods*. Although the heterozygous mutants grew slowly in culture medium containing 200 μg/mL neomycin, the double-knockout strain was unable to grow in growth medium containing 60 μg/mL neomycin and 100 μg/mL hygromycin drug.

Construction of Inducible Gene Expression Strain (LmT7.TR) and Inducible Knockdown Cell Line for HemAC-Lm. A detailed description of the method for the construction of inducible gene expression strain (LmT7.TR) and inducible knockdown cell line for HemAC-Lm is provided in *SI Methods*.

In Vitro Promastigote Growth Profile Analysis. The 10^6 mid–log-phase IKO, CT, OE, and HKO promastigotes were seeded in 10 mL of M199 media and 10% FCS. Growth rates were measured by counting cell number in an improved Neubauer chamber (hemocytometer) at a 24-h interval. Experiments were done in triplicate for each cell type.

Oxygen Consumption Measurement. Oxygen consumption rates were measured using an Oxytherm system (Hansatech Instruments) and Oxygraph plus software at 25 °C, using 0.5 mL of mid–log-phase promastigote suspension (10^8 cells per mL) in PBS solution. All experiments were done in triplicate to minimize the experimental error.

Metacyclic Purification Assay. A detailed description of the method for metacyclic purification by PNA is provided in *SI Methods*.

Parasite Culture Under Hypoxic Environment. Cell viability under hypoxic condition was studied with CT, IKO, HKO, and OE cells using BD Falcon 24-well plates. The 5×10^7 log-phase promastigotes of all cells were centrifuged and washed twice with PBS and were seeded to each well containing 1.0 mL serum-free M199 medium. To achieve hypoxia, a preanalyzed air mixture (95% N_2/5%CO_2; Praxair) was infused into an air chamber (Billups-Rothenberg) constructed with inflow and outflow valves, at a flow rate of 5 L/min for 30 min. The chamber was then sealed and incubated at 22 °C for 12 h (37, 38). The O_2 concentration of sample in hypoxic chamber was measured by Clark-type electrode (Hansatech Instruments). An oxygen electrode demonstrated that the chamber O_2 concentration was less than 12 μM.

Detection of Intracellular cAMP and Measurement of PKA Activity in *L. major* Cells. Intracellular concentration of cAMP in CT, IKO, HKO, and OE cells, incubated at either normoxic or hypoxic condition, were determined by cAMP complete ELISA kit (Enzo Life Sciences). PKA activity was assayed in *L. major* lysates as described by Malki-Feldman and Jaffe (39) by phosphorylation of the specific fluorescent PKA substrate kemptide using the PepTag Non-Radio-active PKA Assay (Promega) kit. A detailed description of these methods is provided in *SI Methods*.

Measurement of Intracellular H_2O_2. For measurement of intracellular H_2O_2 consumption, fluorescence spectrophotometer was used with 2′,7′-dichlorodihydrofluorescein diacetate (DCFDA) as the probe. Cells were washed twice with PBS at 1,200 × *g* (4 °C) for 5 min and incubated with 6 μM DCFDA for 30 min at 26 °C in the dark with mild shaking. The fluorescence intensity was recorded immediately in a fluorescence spectrophotometer at 502 nm for excitation and 529 nm for emission.

Cell Death Assessment by PI and Annexin V Staining. FITC-conjugated annexin V and PI-labeled cells were analyzed by flow cytometer and OlympusIX81 fluorescence microscope. A detailed description of this method is provided in *SI Methods*.

Cell Cycle Analysis. A detailed description of cell cycle analysis by flow cytometer is provided in *SI Methods*.

Measurement of Cellular ATP Content. Intracellular ATP content was measured by a luciferin–luciferase bioluminescence assay using an ATP determination kit (Molecular Probes) according to manufacturer's protocol. ATP concentrations were calculated from the ATP standard curve.

Quantitative Real-Time PCR. Oxidative stress response of CT, HKO, IKO, and OE was analyzed by relative quantification of transcript levels of five important antioxidant genes in *Leishmania*: non-selenium glutathione peroxidase (LmjF.26.0810), iron superoxide dismutaseA (LmjF08.0290), peroxidoxin tryparedoxin peroxidase (LmjF23.0040), superoxide dismutase (LmjF30.2770), and tryparedoxin peroxidase (LmjF.15.1120). A detailed description of this method is provided in *SI Methods*.

Statistical Analysis. All data were expressed as the means ± SD from at least three independent experiments. Statistical analyses for all data were calculated using Student *t* test or analysis of variance wherever applicable using Origin 6.0 software (Microcal Software). The ANOVA was followed by post hoc analysis (multiple-comparison *t* test) for the evaluation of the difference between individual groups. A *P* value of less than 0.05 was considered statistically significant.

ACKNOWLEDGMENTS. We thank Dr. S. M. Beverley (Washington University) for providing pXG-B2863, pXG-neo, and pXG-hyg vectors; Prof. George Cross (The Rockefeller University) for providing pLew13, pLEW82v4, and pLew114hyg5′ vectors; Dr. James D. Bangs (University of Wisconsin–Madison) for *Trypanosoma brucei* Bip antibody; and Dr. A. K. Datta for *Leishmania donovani* adenosine kinase antibody. This work was supported by Council of Scientific and Industrial Research (CSIR) Project BSC 0114, CSIR-Shyama Prasad Mukherjee fellowships (to S.S.S.), CSIR fellowships (to M.B.), University Grants Commission fellowships (to S.M.), and an Indian Council of Medical Research fellowship (to R.S.).

1. Van Hellemond JJ, Tielens AG (1997) Inhibition of the respiratory chain results in a reversible metabolic arrest in Leishmania promastigotes. *Mol Biochem Parasitol* 85(1):135–138.
2. Van Hellemond JJ, Van der Meer P, Tielens AGM (1997) Leishmania infantum promastigotes have a poor capacity for anaerobic functioning and depend mainly on respiration for their energy generation. *Parasitology* 114(4):351–360.
3. Sasakura Y, Yoshimura-Suzuki T, Kurokawa H, Shimizu T (2006) Structure-function relationships of EcDOS, a heme-regulated phosphodiesterase from Escherichia coli. *Acc Chem Res* 39(1):37–43.
4. Gilles-Gonzalez MA, Gonzalez G (2005) Heme-based sensors: Defining characteristics, recent developments, and regulatory hypotheses. *J Inorg Biochem* 99(1):1–22.
5. Ferguson-Miller S, Babcock GT (1996) Heme/copper terminal oxidases. *Chem Rev* 96(7):2889–2908.
6. Antonini E, Brunori M (1971) *Hemoglobin and Myoglobin in Their Reactions with Ligands* (Elsevier/North-Holland Biomedical, Amsterdam), 436 pp.
7. Hou S, et al. (2000) Myoglobin-like aerotaxis transducers in Archaea and Bacteria. *Nature* 403(6769):540–544.
8. Agarwal N, Lamichhane G, Gupta R, Nolan S, Bishai WR (2009) Cyclic AMP intoxication of macrophages by a Mycobacterium tuberculosis adenylate cyclase. *Nature* 460(7251): 98–102.
9. Botsford JL, Harman JG (1992) Cyclic AMP in prokaryotes. *Microbiol Rev* 56(1): 100–122.
10. Chen Y, et al. (2000) Soluble adenylyl cyclase as an evolutionarily conserved bicarbonate sensor. *Science* 289(5479):625–628.
11. Jaiswal BS, Conti M (2003) Calcium regulation of the soluble adenylyl cyclase expressed in mammalian spermatozoa. *Proc Natl Acad Sci USA* 100(19):10676–10681.
12. Berthet J, Rall TW, Sutherland EW (1957) The relationship of epinephrine and glucagon to liver phosphorylase. IV. Effect of epinephrine and glucagon on the reactivation of phosphorylase in liver homogenates. *J Biol Chem* 224(1):463–475.
13. Bhattacharya A, Biswas A, Das PK (2008) Role of intracellular cAMP in differentiation-coupled induction of resistance against oxidative damage in Leishmania donovani. *Free Radic Biol Med* 44(5):779–794.
14. Salmon D, et al. (2012) Adenylate cyclases of Trypanosoma brucei inhibit the innate immune response of the host. *Science* 337(6093):463–466.
15. Bashford D, Chothia C, Lesk AM (1987) Determinants of a protein fold. Unique features of the globin amino acid sequences. *J Mol Biol* 196(1):199–216.
16. Tucker CL, Hurley JH, Miller TR, Hurley JB (1998) Two amino acid substitutions convert a guanylyl cyclase, RetGC-1, into an adenylyl cyclase. *Proc Natl Acad Sci USA* 95(11): 5993–5997.
17. Horecker BL (1943) The absorption spectra of hemoglobin and its derivatives in the visible and near infra-red regions. *J Biol Chem* 148(1):173–183.
18. Fago A, et al. (2004) Allosteric regulation and temperature dependence of oxygen binding in human neuroglobin and cytoglobin. Molecular mechanisms and physiological significance. *J Biol Chem* 279(43):44417–44426.
19. Acin-Perez R, et al. (2009) Cyclic AMP produced inside mitochondria regulates oxidative phosphorylation. *Cell Metab* 9(3):265–276.
20. Pawelek J, Halaban R, Christie G (1975) Melanoma cells which require cyclic AMP for growth. *Nature* 258(5535):539–540.
21. Brønstad GO, Sand TE, Christoffersen T (1983) Bidirectional concentration-dependent effects of glucagon and dibutyryl cyclic AMP on DNA synthesis in cultured adult rat hepatocytes. *Biochim Biophys Acta* 763(1):58–63.
22. Sacks DL, Perkins PV (1984) Identification of an infective stage of Leishmania promastigotes. *Science* 223(4643):1417–1419.
23. Pal S, Dolai S, Yadav RK, Adak S (2010) Ascorbate peroxidase from Leishmania major controls the virulence of infective stage of promastigotes by regulating oxidative stress. *PLoS ONE* 5(6):e11271.
24. Vassella E, Reuner B, Yutzy B, Boshart M (1997) Differentiation of African trypanosomes is controlled by a density sensing mechanism which signals cell cycle arrest via the cAMP pathway. *J Cell Sci* 110(Pt 21):2661–2671.
25. Dolai S, Yadav RK, Pal S, Adak S (2009) Overexpression of mitochondrial Leishmania major ascorbate peroxidase enhances tolerance to oxidative stress-induced programmed cell death and protein damage. *Eukaryot Cell* 8(11):1721–1731.
26. Leist M, Single B, Castoldi AF, Kühnle S, Nicotera P (1997) Intracellular adenosine triphosphate (ATP) concentration: A switch in the decision between apoptosis and necrosis. *J Exp Med* 185(8):1481–1486.
27. Duranteau J, Chandel NS, Kulisz A, Shao Z, Schumacker PT (1998) Intracellular signaling by reactive oxygen species during hypoxia in cardiomyocytes. *J Biol Chem* 273(19):11619–11624.
28. Kim HP, Roe JH, Chock PB, Yim MB (1999) Transcriptional activation of the human manganese superoxide dismutase gene mediated by tetradecanoylphorbol acetate. *J Biol Chem* 274(52):37455–37460.
29. Sugino N, Karube-Harada A, Sakata A, Takiguchi S, Kato H (2002) Different mechanisms for the induction of copper-zinc superoxide dismutase and manganese superoxide dismutase by progesterone in human endometrial stromal cells. *Hum Reprod* 17(7):1709–1714.
30. Hong SK, Cha MK, Choi YS, Kim WC, Kim IH (2002) Msn2p/Msn4p act as a key transcriptional activator of yeast cytoplasmic thiol peroxidase II. *J Biol Chem* 277(14): 12109–12117.
31. Gilles-Gonzalez MA, Ditta GS, Helinski DR (1991) A haemoprotein with kinase activity encoded by the oxygen sensor of Rhizobium meliloti. *Nature* 350(6314):170–172.
32. Chang AL, et al. (2001) Phosphodiesterase A1, a regulator of cellulose synthesis in Acetobacter xylinum, is a heme-based sensor. *Biochemistry* 40(12):3420–3426.
33. Dioum EM, et al. (2002) NPAS2: A gas-responsive transcription factor. *Science* 298(5602):2385–2387.
34. Tuckerman JR, et al. (2009) An oxygen-sensing diguanylate cyclase and phosphodiesterase couple for c-di-GMP control. *Biochemistry* 48(41):9764–9774.
35. Mukherjee S, et al. (2012) NAD(P)H cytochrome b5 oxidoreductase deficiency in Leishmania major results in impaired linoleate synthesis followed by increased oxidative stress and cell death. *J Biol Chem* 287(42):34992–35003.
36. Dolai S, Yadav RK, Pal S, Adak S (2008) Leishmania major ascorbate peroxidase overexpression protects cells against reactive oxygen species-mediated cardiolipin oxidation. *Free Radic Biol Med* 45(11):1520–1529.
37. Kim KS, et al. (1998) Protection from reoxygenation injury by inhibition of rac1. *J Clin Invest* 101(9):1821–1826.
38. Martinive P, et al. (2006) Preconditioning of the tumor vasculature and tumor cells by intermittent hypoxia: Implications for anticancer therapies. *Cancer Res* 66(24): 11736–11744.
39. Malki-Feldman L, Jaffe CL (2009) Leishmania major: Effect of protein kinase A and phosphodiesterase activity on infectivity and proliferation of promastigotes. *Exp Parasitol* 123(1):39–44.